SUPPLEMENT

POLSTRACC

Airborne Experiment for Studying the Polar Stratosphere in a Changing Climate with the High Altitude and Long Range Research Aircraft (HALO)

Hermann Oelhaf, Björn-Martin Sinnhuber, Wolfgang Woiwode, Harald Bönisch, Heiko Bozem, Andreas Engel, Andreas Fix, Felix Friedl-Vallon, Jens-Uwe Grooß, Peter Hoor, Sören Johansson, Tina Jurkat-Witschas, Stefan Kaufmann, Martina Krämer, Jens Krause, Erik Kretschmer, Dominique Lörks, Andreas Marsing, Johannes Orphal, Klaus Pfeilsticker, Michael Pitts, Lamont Poole, Peter Preusse, Markus Rapp, Martin Riese, Christian Rolf, Jörn Ungermann, Christiane Voigt, C. Michael Volk, Martin Wirth, Andreas Zahn, and Helmut Ziereis

This document is a supplement to "POLSTRACC: Airborne Experiment for Studying the Polar Stratosphere in a Changing Climate with the High Altitude and Long Range Research Aircraft (HALO)," Hermann Oelhaf, Björn-Martin Sinnhuber, Wolfgang Woiwode, Harald Bönisch, Heiko Bozem, Andreas Engel, Andreas Fix, Felix Friedl-Vallon, Jens-Uwe Grooß, Peter Hoor, Sören Johansson, Tina Jurkat-Witschas, Stefan Kaufmann, Martina Krämer, Jens Krause, Erik Kretschmer, Dominique Lörks, Andreas Marsing, Johannes Orphal, Klaus Pfeilsticker, Michael Pitts, Lamont Poole, Peter Preusse, Markus Rapp, Martin Riese, Christian Rolf, Jörn Ungermann, Christiane Voigt, C. Michael Volk, Martin Wirth, Andreas Zahn, and Helmut Ziereis (*Bull. Amer. Meteor. Soc.*, **100,** 2634–2663) • ©2019 American Meteorological Society • *Corresponding authors:* Hermann Oelhaf, hermann.oelhaf@kit.edu; Björn-Martin Sinnhuber, bjoern-martin.sinnhuber@kit.edu • DOI:10.1175/BAMS-D-18-0181.2

PAYLOAD DESCRIPTION. *Remote sensing instruments.* GLORIA.[1] The imaging Fourier transform spectrometer GLORIA provides two- and three-dimensional vertically and horizontally highly resolved distributions of trace gases, temperature, and cloud parameters around and below flight altitude (Friedl-Vallon et al. 2014; Riese et al. 2014). The instrument was operated in two different observation modes: The "chemistry mode" is optimized to high spectral sampling at a constant viewing angle, typically perpendicular to the heading of the aircraft, allowing the retrieval of a comprehensive set of minor species (i.e., HNO_3, $ClONO_2$, H_2O, O_3, CFCs, C_2H_6, PAN, among many others). Individual vertical profiles are combined to curtains across the flight track with an along-track sampling of about 3 km and a vertical resolution of typically 500 m. Combined (systematic and random) errors are estimated to be in the range of 1–2 K for temperature, and 10%–20% for trace gases (Johansson et al. 2018). The fast and spectrally less resolved "dynamics mode" is optimized to 2D and 3D high-spatial-resolution observations of temperature and more abundant species (e.g., O_3, HNO_3, CFC-12) for investigating dynamic structures such as gravity waves, utilizing tomographic approaches (Ungermann et al. 2010).

Mini-DOAS. The mini-DOAS instrument is an ultraviolet (UV)–visible (VIS)–near-infrared (NIR) six-channel optical spectrometer by which scattered skylight received from scanning limb and nadir directions can be analyzed. The postflight analysis of the collected data for the detection of O_3, O_4, NO_2, OClO, and BrO includes a DOAS (Differential Optical Absorption Spectroscopy; Platt and Stutz 2008) analysis of the measured limb spectra with settings as described in detail in Hüneke et al. (2017)

[1] See the appendix for a list of abbreviations and acronyms.

and Werner et al. (2017). For the retrieval of absolute concentrations at flight altitude the recently developed O_3-scaling method is used, of which the details are discussed in Stutz et al. (2017) and Hüneke et al. (2017). For the method the radiative transfer of each limb measurement is forward modeled using the Monte Carlo radiative transfer (RT) model McArtim (Deutschmann et al. 2011) considering the atmospheric, instrumental, and celestial (e.g., sun position) parameters and geolocation.

Typical precision errors of the combined methods are ±5 ppb for O_3, ±10 ppt for NO_2, <±0.25 ppt for OClO somewhat depending on the solar zenith angle, and ±0.5 ppt for BrO. Finally, systematic errors in the individual absorption cross section need to be added to the precision error. These are for O_3-UV ± 1.3%, O_3-vis ± 2%, NO_2 ± 2%, OClO ± 10%, and BrO ±10% [for the absorption cross-section errors see Burkholder et al. (2015) and for the total error budget of the mini-DOAS measurements see Hüneke et al. (2017)].

WALES. WALES is an airborne multiwavelength H_2O–O_3 Differential Absorption Lidar (DIAL) with additional channels for aerosol and cloud characterization developed by the German Aerospace Center (DLR; Wirth et al. 2009). It can be operated in different configurations with ozone capability or as multiline water vapor DIAL, in upward- or downward-pointing mode. For POLSTRACC the upward-pointing configuration with H_2O measurement on one absorption line, but with an additional ozone channel was installed. Water vapor is measured at 935 nm and ozone at 305 nm.

Additional channels at 1064 and 532 nm with depolarization capability allow for the characterization of aerosol and cloud particles. At 532 nm an additional high-spectral-resolution channel is used to directly measure the optical thickness without further assumptions about the scattering phase functions of the particles under consideration. Laser pulses are emitted at a repetition rate of 100 Hz, but the output data rate is reduced to 5 Hz by onboard signal processing and further by offline processing.

For the aerosol and cloud channels the typical horizontal resolution of the final products for POLSTRACC is 20 s, corresponding to a horizontal resolution of 4 km. For water vapor and ozone, the resolution is further reduced to 16 km to achieve a low statistical noise of about 5% in the first 10 km of range. The vertical resolution is 15 m for the aerosol/cloud channels and 500 m for water vapor and ozone

In situ instruments. AENEAS. The AENEAS instrument is a two-channel instrument for the simultaneous detection of nitrogen oxide (NO) and the sum of all reactive nitrogen species (NO_y). It is based on the chemiluminescence detection of NO in combination with a gold converter technique for NO_y measurements. Its time resolution is 1 s. This instrument was previously successfully operated during several missions, for example, POLSTAR (Ziereis et al. 2000) and INCA (Ziereis et al. 2004), as well as other recent HALO missions (TACTS/ESMVal, ML-CIRRUS, ACRIDICON, WISE). The overall uncertainty of the measurement depends on the observed concentration level. It is about 8% for volume mixing ratios of 0.5 nmol mol^{-1} and about 6.5% for 1 nmol mol^{-1} (Stratmann et al. 2016).

During POLSTRACC the instrument was configured in a way to simultaneously measure gas-phase and particulate nitrate. The two channels of the detector have been connected to a forward- and backward-facing inlet. The backward-facing inlet does not allow for the sampling of ice particles. The forward-facing inlet samples particles with enhanced efficiency with respect to the gas phase. This experimental approach was already used during former missions like INCA (Ziereis et al. 2004).

AIMS. The Atmospheric Ionization Mass Spectrometer (AIMS; Jurkat et al. 2016) provides accurate measurements of the important chlorine reservoirs HCl and $ClONO_2$, as well as of HNO_3, HONO, and SO_2 (Jurkat et al. 2014; Voigt et al. 2014), in order to study heterogeneous chemical processes associated to PSCs and cirrus clouds. The trace gases are ionized using SF_5^- ions (Jurkat et al. 2010) and the resultant product ions are detected with a linear quadrupole mass spectrometer. The instrument is calibrated in flight. The AIMS measurements are performed at a 1.7-s time resolution corresponding to ~350-m horizontal resolution (Jurkat et al. 2017). A 17-s running average yields detection limits <12 parts per trillion by volume (pptv) and 10%–15% precision (12%–20% accuracy) for HCl and $ClONO_2$.

BAHAMAS. The Basic HALO Measurement And Sensor System (BAHAMAS) belongs to the basic instrumentation of the aircraft and consists of a data acquisition with interfaces into the aircraft systems and a suite of own sensors (Krautstrunk and Giez 2012). The prominent air data (nose) boom on HALO is part of the system and carries a pressure and airflow sensor. BAHAMAS measures basic meteorological and aerodynamic data including temperature, pressure, and the three-dimensional wind vector as well as aircraft state parameters like position, attitude, and aircraft speed. The data are recorded with a time resolution of 100 Hz. The standard output after post processing

is 10 Hz. BAHAMAS also provides a comprehensive user infrastructure including a local network, quicklook data streaming, a reference time standard, and the recorded video signals from the aircraft camera system along with a communication and data link between onboard instrument operators and the ground teams.

Dropsonde system. The dropsonde system (Voigt et al. 2017) uses Vaisala sonde type RD94. Meteorological data are recorded with a GPS receiver with a custom-made firmware and include vertical profiles of pressure, temperature, humidity, and wind.

FAIRO. The Fast and Accurate In Situ Ozone Instrument (FAIRO) combines a fast and precise chemiluminescence detector and an accurate dual-beam UV photometer for accurate high-resolution ozone observations. Both instruments work at the physical limit (photon-noise limited). The total uncertainty is 1.5% and the typical precision is 0.5% at 10 Hz (Zahn et al. 2012).

FISH. The Fast In Situ Stratospheric Hygrometer (FISH) detects water vapor based on the Lyman-alpha photofragment fluorescence technique (Zöger et al. 1999). It has been deployed on various platforms for almost two decades for high-precision measurements of water vapor in the UTLS and its measurements of H_2O have been validated with several in situ instruments and within laboratory studies (Meyer et al. 2015). Measurements are recorded at a temporal resolution of 1 s with a precision of 1% + 0.35 ppmv and an accuracy of 5.3%.

GhOST-MS. The GC-MS-system GhOST-MS measures a large set of halogenated chemical tracers (e.g., CH_3I, CH_3Br, CH_2Br_2, halons, and CFCs) using negative chemical ionization (Sala et al. 2014) with a time resolution of 4 min and a precision down to 0.5%. In a second channel an electron capture detector measures CFC-12 and SF_6 with a time resolution of 1 min and a precision of about 0.2% for CFC-12 and 0.7% for SF_6. The trace gases observed by GhOST-MS have a wide span of chemical lifetimes reaching from several days to many years, allowing investigations of chemical processes (e.g., halogen budget; see Sala et al. 2014) and transport processes on time scales from days to years, including mean age determination (e.g., Bönisch et al. 2011; Engel et al. 2006).

HAGAR-V. HAGAR-V is a novel five-channel tracer system for HALO operated for the first time during POLSTRACC. The instrument combines a fast and precise CO_2 measurement by a nondispersive infrared (NDIR) analyzer, a two-channel GC-ECD-system, and a two-channel GC-MS-system. The package is calibrated in situ every several minutes during the flight to guarantee stability and high precision. In addition to CO_2 at time resolution of 1–3 s and precision of ~0.1 ppm, HAGAR-V provides long-lived tracers (SF_6, CH_4, N_2O, CFC-11, CFC-12) every 90 s by GC/ECD as well as a suite of short-lived chlorinated hydrocarbons by GC-MS every 90–180 s, depending on configuration, all with precisions on the order of 1% and accuracy <2%. HAGAR-V is a modernized and extended version of the very successful HAGAR system that has been regularly deployed aboard the M55 Geophyisca aircraft since 1998 (e.g., Werner et al. 2010).

HAI. HAI is a fully autonomous, airborne hygrometer for atmospheric investigations for simultaneous gas-phase and total H_2O detection on the HALO aircraft. HAI employs first-principle, direct, tunable diode laser absorption spectroscopy (dTDLAS) for calibration-free, absolute H_2O detection. HAI simultaneously measures at 1.4 and 2.6 μm and in closed-path and open-path configurations, respectively, covers a H_2O range of 1–40,000 ppmv at up to 1.4-ms time resolution, and achieves precisions of 0.18 and 0.055 ppmv at 1.4 and 2.6 μm, respectively (Buchholz et al. 2017).

TRIHOP. The TRIHOP instrument is a three-channel quantum cascade laser infrared absorption spectrometer, which has been successfully operated onboard HALO during TACTS/ESMVal (Müller et al. 2016) and OMO (Lelieveld et al. 2018). During POLSTRACC, the instrument was used to measure CO, N_2O, and CH_4 with an integration time of 1.5 s for each channel, resulting in a time resolution of 7 s per species. The instrument is in situ calibrated against secondary standards of compressed ambient air, which are compared against NOAA primary standards before and after the campaign. During POLSTRACC, the instrument achieved a precision (2σ) of 1.15, 1.84, and 9.46 ppbv for CO, N_2O, and CH_4, respectively (Krause et al. 2018) with a total uncertainty of 2.3, 2.7, and 13.7 ppbv, respectively.

WARAN. The WARAN (Water Vapor Analyzer) instrument consists of the tunable diode laser instrument WVSS-II (SpectraSensors Inc., United States) to measure total or gas-phase water (Kaufmann et al. 2014). The instrument is integrated in the AIMS rack, connected to a forward-facing inlet and actively pumped to achieve defined flow conditions in the inlet for sampling total water in clouds and gas-phase water out of clouds (Kaufmann et al. 2016). The instrument was calibrated on the ground using a dewpoint mirror

(MBW 373LX) as reference. This led to a detection limit <10 ppmv for tropospheric water vapor measurements. During POLSTRACC, the instrument was mainly used to detect the cloud's ice water content (IWC). Due to particle enhancement in the instrument's inlet by factors of 20–35, the detection limit for IWC is significantly lower (0.3–0.5 ppmv) and allows for the quantification of IWC in most clouds except very thin cirrus (Kaufmann et al. 2018).

COOPERATING SATELLITE PROJECTS. Tight cooperation was realized with the CALIOP and MLS teams, both during the campaign and for data analysis.

MLS. The Microwave Limb Sounder (MLS; e.g., Waters et al. 2006) aboard the NASA Earth Observing System *Aura* satellite is the successor of the MLS instrument on the Upper Atmosphere Research Satellite (UARS). The *Aura* satellite flies together with (among others) the *CALIPSO* satellite in the A-Train constellation with a 1345 local equator-crossing time at an orbit altitude of 705 km. Measurements are recorded between 82°S and 82°N every 165 km along the sun-synchronous orbit. MLS provides vertically resolved volume mixing ratios of trace gases, such as O_3, HNO_3, HCl, ClO, and N_2O. Characteristics of these measurements are given by Livesey et al. (2018).

CALIOP. The Cloud-Aerosol Lidar with Orthogonal Polarization (CALIOP), the primary instrument on the *CALIPSO* satellite, is a dual-wavelength polarization-sensitive lidar that provides high-vertical-resolution profiles of backscatter coefficients at 532 and 1064 nm. The unique capability of the CALIOP spaceborne lidar is to probe clouds and aerosols at very high spatial resolution. Although CALIOP is not specifically designed for stratospheric applications, PSCs generally produce detectable enhancements in CALIOP backscatter profiles. The CALIOP measurements of the 532-nm perpendicular backscatter coefficient provide additional information on particle shape, from which PSC composition can be inferred. The *CALIPSO* satellite was launched 2006 and flies in a 98° inclination orbit at 705-km altitude, together (among others) with the Aura satellite in the NASA A-Train constellation. A detailed discussion of the CALIOP PSC climatology including the cold periods of winter 2015/16 is given by Pitts et al. (2018).

PLANNING, IMPLEMENTATION, EXECUTION, AND REPORTING OF SCIENCE FLIGHTS. Detailed scientific flight planning made use of a dedicated mission support tool (MSS, Mission Support System; Rautenhaus et al. 2012) that was extended and adapted to the POLSTRACC needs. Forecast products were based on ECMWF deterministic forecasts and chemical transport model forecasts with CLaMS (Grooß et al. 2014). CLaMS model forecasts included distribution of essential tracers and chemically active species (e.g., O_3, HNO_3, photochemically active nitrogen and halogen species), as well as cirrus occurrence and properties such as ice water content (cf. "Modeling activities" section in main text). In addition to maps on isentropic or pressure levels, CLaMS forecasts were also available as vertical "curtains" along the planned flight path.

Selected flight plans were then presented and discussed in the daily meteorological and flight planning briefings and via the internet. Science meetings were organized roughly on a weekly basis with more extensive discussions toward the end of each mission phase.

The final decision on actual flights (routes, flights levels, duration) was based on operational constraints (instrument readiness, HALO performance, team duty times, surface weather expected for takeoff and touchdown including alternates, air traffic control issues, etc.) and science requirements derived from the scientific flight plan.

Figure ES1a presents an example of the first page of the "Flight Plan" for a polar survey flight conducted on 20 January 2016 under very cold conditions, underflying the cold pool and the vortex core. Figures ES1b and ES1c show forecasted cloud cover and potential vorticity based on ECMWF forecasts along the projected flight path. A collage of forecasted maps of O_3, DNO_y (NO_y* minus NO_y), ClO_x, and equivalent latitude at the 150 hPa level is shown in Fig. ES2.

During flights, scientists on the ground were able to follow closely the mission, and in many cases, live-streaming of crucial instrumental status and quick-look data were feasible via satellite connection (INMARSAT and IRIDIUM). A chat function allowed some troubleshooting and adapting the flight plan to updated information or in case of air traffic control (ATC) demands. Data-reduced maps or software patches could be uploaded from ground if necessary.

Flight reports were written after each scientific flight, summarizing main findings, including special observations and events, as well as instrument statuses.

COMPILATION OF SCIENTIFIC FLIGHTS. Tables 2–4 in the main text contain characteristic data of all PGS flights phase by phase and flight by flight. Here we outline basic goals and special observations of each flight and refer to associated figures in the

(a)

Flight Name: **PGS_08_20160120**
Flight Date: 20.01.2016
Flight Template Date: 19.01.2016
Flight Template Version: 01

Main Objectives:
- Arctic survey:
- Low temperatures with $T<T_{NAT}$ off Greenland coast near point „D"
- Look for possible tropospheric tracer signatures in lower stratosphere along Greenland coast
- GLORIA tracer measurements along transsects in polar air masses
- Look for possibe enhancements of NOy
- Investigate tropopause fold structures with drop sondes and GLORIA along A-B and F-G

Operations:
10:15 --- preflight briefing at aircraft; go/no go for roll-out
10:55 --- all instruments off, except TRIHOP, AIMS, FISH, GhOST, HAGAR
10:55 --- TRIHOP, AIMS, FISH, GhOST, HAGAR wait for notice to switch off
10:55 --- hangar door open, HALO door closed; notice for power off then 5 min to shut down remaining instruments
11:00 --- power off, roll-out (operators TRIHOP, AIMS, FISH, GhOST, HAGAR, FX staff stay onboard during roll-out)
11:05 --- APU on, mission power on
11:15 --- fueling
11:55 --- everyone not flying leaves aircraft
12:15 --- Take-off (flight time ~09:10)
21:25 --- expected landing, 30 min APU power on apron
21:55 --- power off, aircraft in hangar
22:05 --- power on in hangar
22:05 --- de-briefing (in hangar)

POLSTRACC/GW-LCYCLE/SALSA

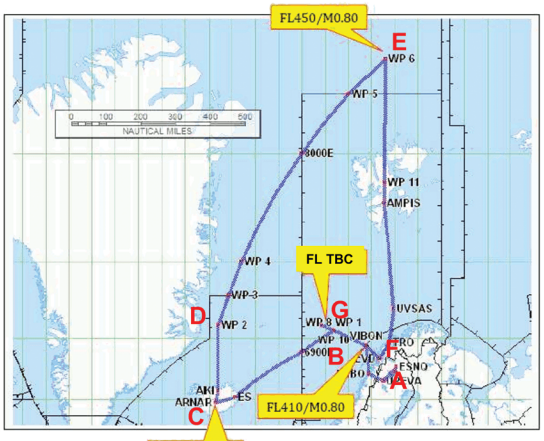

Major Waypoints:

A	ENSQ	67°49'N	20°20'E
B	WP1	70°36'N	07°00'E
C	ARNAR	64°14'N	18°33'W
D	WP2	71°00'N	18°00'W
E	WP6	83°00'N	18°00'E
F	Evenes	68°27'N	16°41'E
G	WP8	70°36'N	07°00'E
	ENSQ	67°49'N	20°20'E

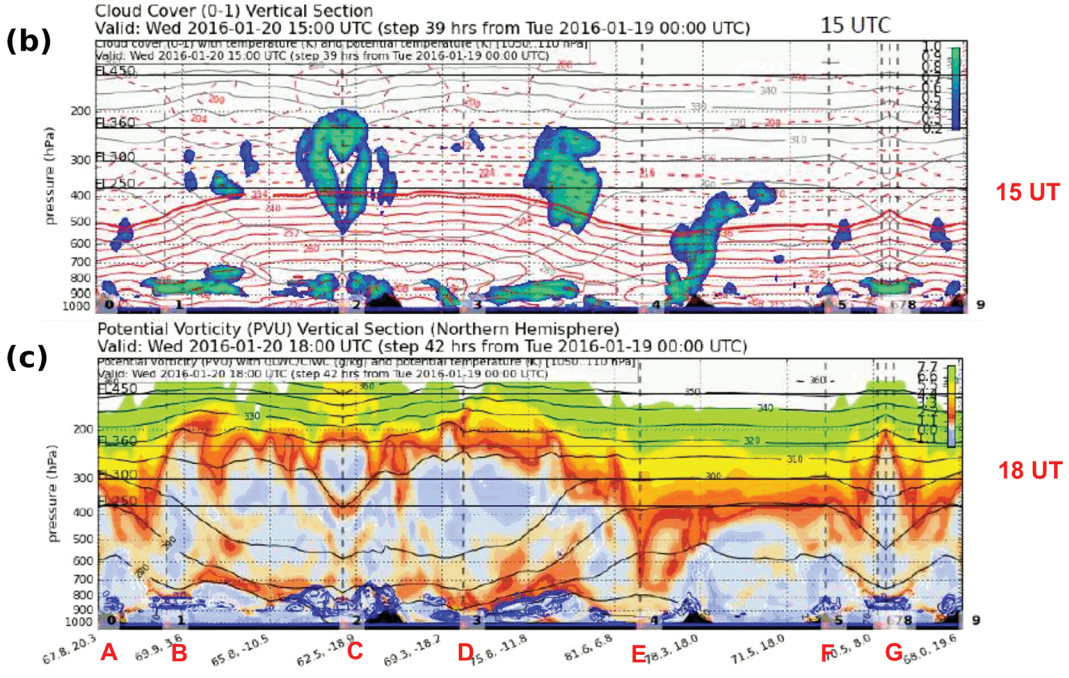

Fig. ES1. (a) Flight plan for research flight PGS-08 conducted on 20 Jan 2016 with major waypoints; (b) cloud cover and (c) potential vorticity for the projected flight path based on ECMWF operational forecasts. Note the complex structure of the tropopause with a tropopause fold at waypoint E.

"Highlighted results" section of the main text of the main paper and to relevant publications. For each flight, the flight path is illustrated on a map with ECMWF potential temperatures at typical HALO cruise altitude of 13 km along with a vortex indicator.

Mission phase 1: Early winter. PGS-04—17 December 2015: SALSA-flight-1. The goal of this flight (Fig. ES3) was to access a wide range of equivalent latitudes and potential temperatures by horizontally crossing the tropopause at a high altitude, and reaching a

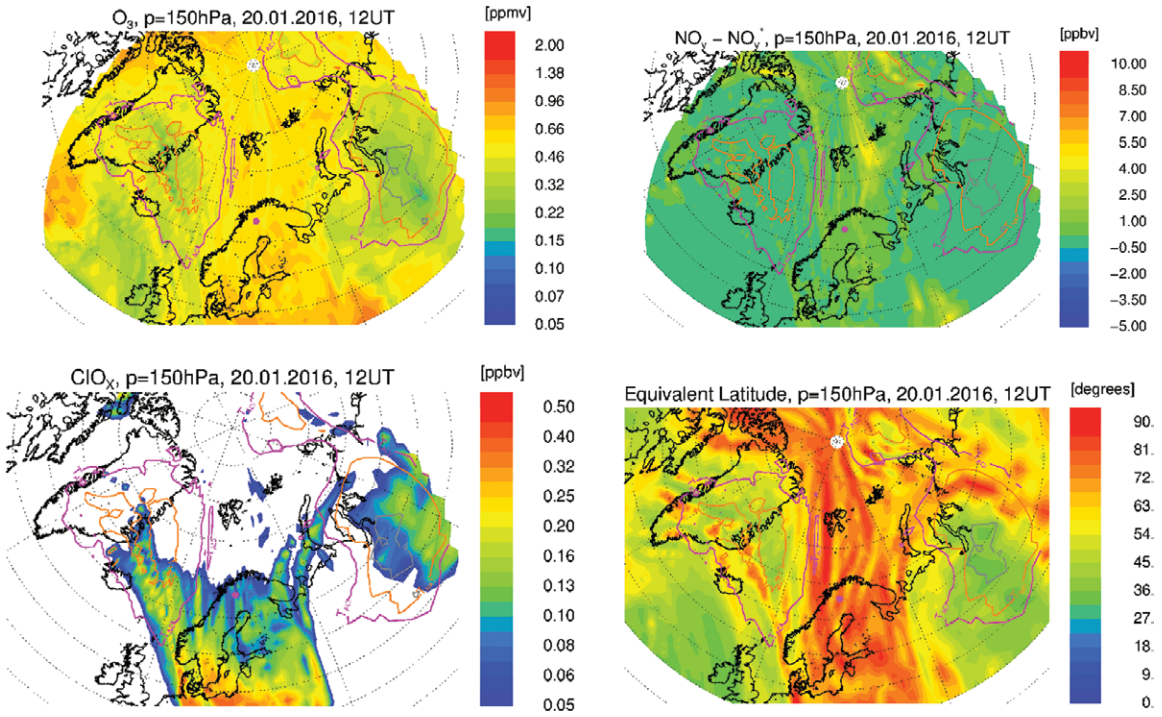

Fig. ES2. CLAMS forecast maps of (top left) O_3, (top right) ΔNO_y (=NO_y – NO_y*, see text), (bottom left) ClO_x, and (bottom right) equivalent latitude for PGS-08 for the pressure level of 150 hPa (corresponding to the predicted cruising pressure altitude of HALO).

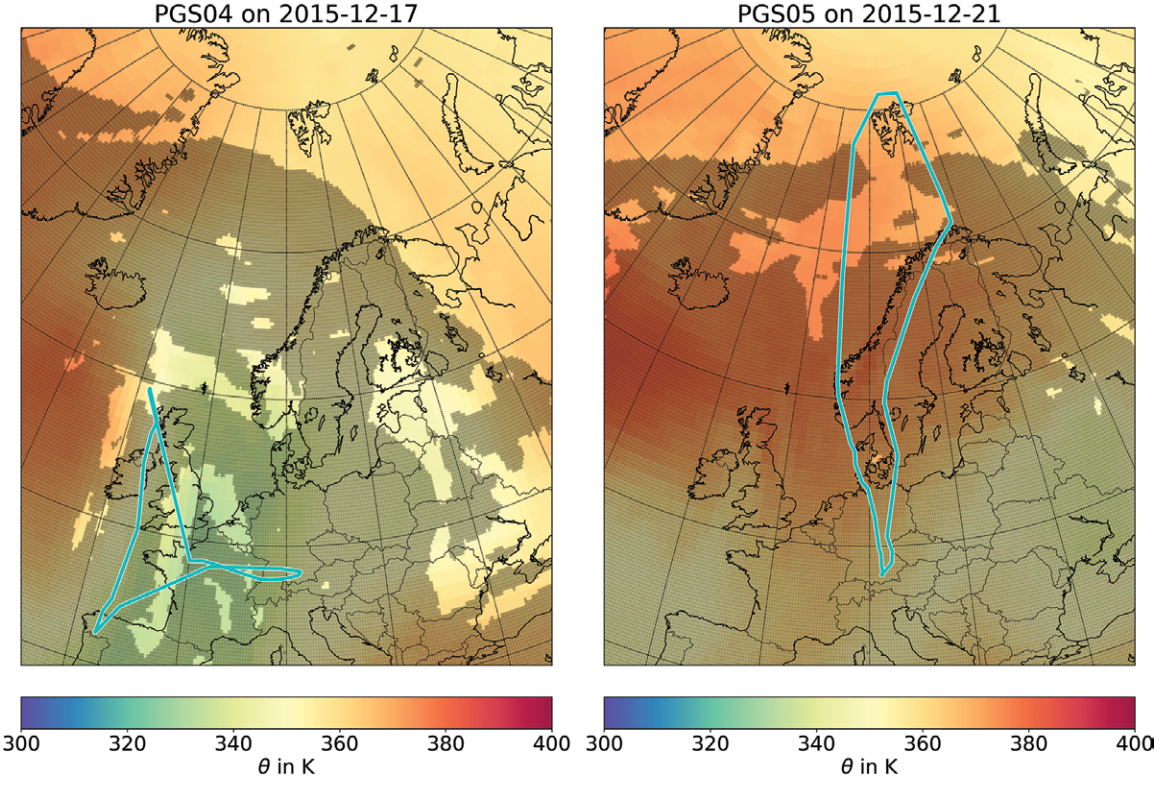

Fig. ES3. The flight paths for PGS-04 and PGS-05 (cyan) on a map with ECMWF potential temperatures (shading) at a typical HALO cruise altitude of 13 km. Regions outside the polar vortex [according to Nash et al. (1996) at θ = 370 K] are marked with a gray shadow.

stratospheric filament north of Ireland. This flight was primarily devoted to SALSA objectives.

PGS-05—21 December 2015: Early winter survey flight. This flight (Fig. ES3) aimed at a survey of the early polar vortex accessing 81°N by heading north over the North Atlantic, flying around Spitsbergen clockwise, and passing Scandinavia on the way back to Germany. The vortex edge was located south of Spitsbergen. Vortex filaments were crossed over Scandinavia. Overall, the flight provided two long transects from 48° to 81°N. Coordinated observations with an ozone sonde launched in Ny-Ålesund and the WALES lidar were used for cross validation (see Fig. 7 in main text).

Mission phase 2: Midwinter. PGS-06—12 January 2016: Transfer flight to Kiruna. The day of the ferry flight PGS-06 (Fig. ES4), the fully developed vortex

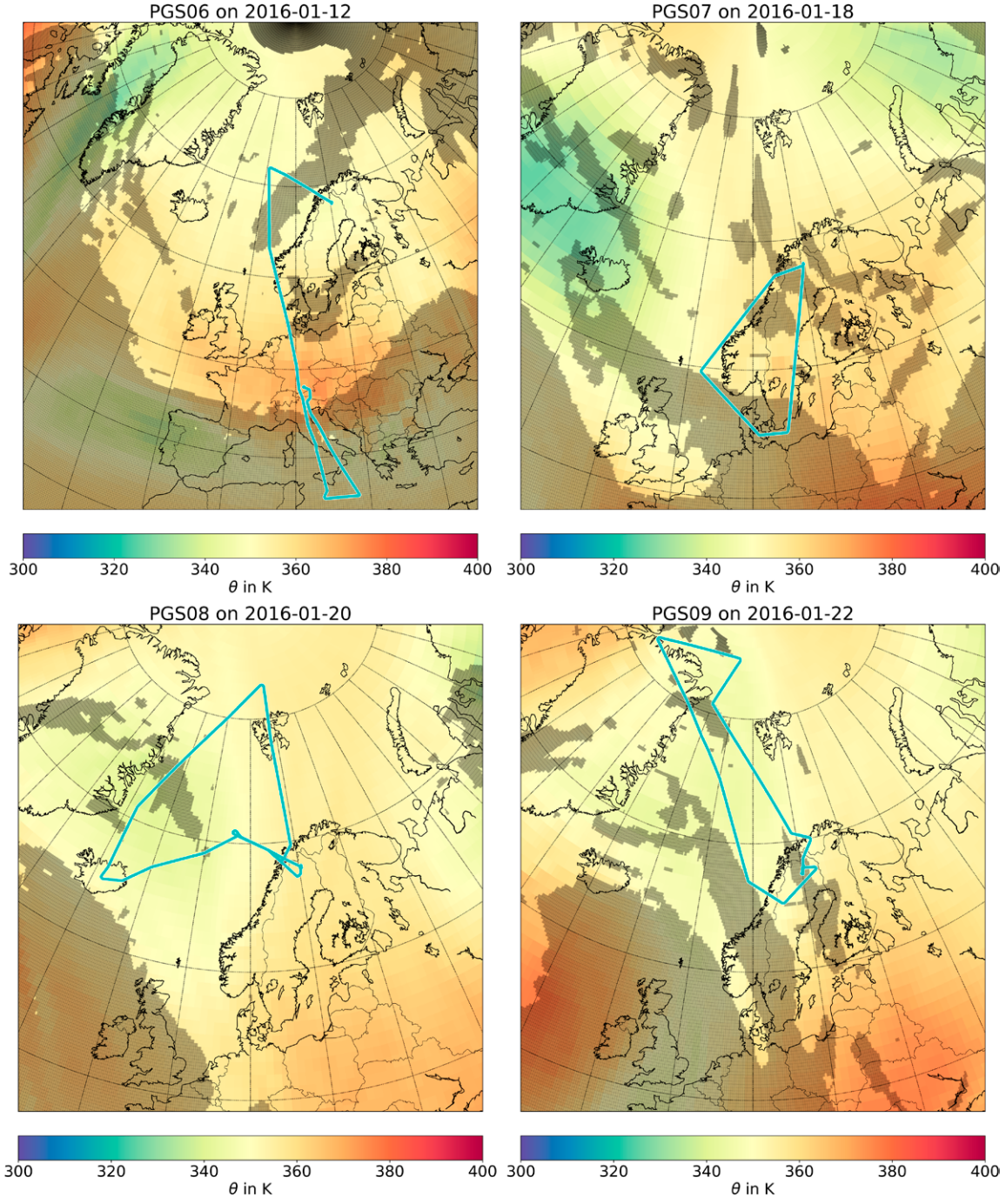

Fig. ES4. As in Fig. ES3, but for flights PGS-06–PGS-09.

showed a southward stretching slope toward middle Europe in conjunction with a strong polar-front jet stream located over the Alps. For this reason, before heading to Kiruna, a detour of the transfer flight to the southern Mediterranean (turning point at ~35°N) was realized crossing the vortex edge and the polar front jet stream and reaching subtropical air masses with O_3 VMRs lower than 100 ppbv in contrast to up to 1300 ppbv in the lowermost stratosphere above central Europe. The tropopause fold associated to the jet stream with propagating mountain waves has been studied in detail by Woiwode et al. (2018), indicating deep intrusions of dry ozone-rich stratospheric air (cf. Fig. 10 in main text). Enhanced HNO_3 at the bottom of the vortex was detected by GLORIA indicating nitrification of the LMS (see Johansson et al. 2018; Braun et al. 2019). In the end, the flight provided a long transect covering latitudes from 35° to 72°N from subtropical air masses to air masses characteristic of the bottom of the vortex core and cold pool.

PGS-07—18 January 2016: Local flight from Kiruna to probe forecasted renitrification and chlorine activation. CLaMS forecast runs indicated enhanced NO_y and activated chlorine in the LMS at the edge of the vortex over southern Scandinavia. Accordingly, the flight plan (Fig. ES4) was set up to probe activated air masses with enhanced ClO_x and NO_y supposedly due to renitrification and to cross a streamer with high N_2O/low O_3 over the southernmost leg.

Several layers of enhanced nitric acid were encountered at FL 450. At the uppermost FL 470 sharp enhancements of particulate NO_y were measured by the NO_y channel of AENEAS with the forward facing inlet. These "spikes," previously identified as NAT particles, were observed for more than 1 h at temperatures of 204 K or above flying along the coast of Norway (H. Ziereis et al. 2019, unpublished manuscript). Visually a faint cloud layer was observed from the cockpit above HALO. In the distance, a silver cloud layer suggested a PSC cloud. Enhanced values of NO_y and HNO_3 were accompanied by strongly activated chlorine, as identified by the discrepancy between measured HCl, $ClONO_2$ and estimated Cl_y (Marsing et al. 2019).

PGS-08—20 January 2016: Polar survey flight east of Greenland with PSC observation. This flight (Fig. ES4) was devoted to providing a survey of PSC distribution in the area between Greenland, Iceland, Spitsbergen, and Scandinavia. At this day, the cold pool of the vortex was situated between Greenland and the Norwegian sea west of Scandinavia. Objectives were to search for model-predicted renitrification north of Scandinavia, enhanced ClO_x northeast of Iceland, and encounter at flight level cold temperatures east of Greenland with possible PSCs reaching down to flight levels. Dropsondes were released for temperature comparison with GLORIA below flight level. In addition, the development of an interesting tropopause fold west of Norway in coordination with the Falcon aircraft was studied.

East of Greenland, the minimum temperature at a flight level of –76°C was reached. Evidence of ongoing nitrification of the Arctic LMS was observed by GLORIA, reaching up to 7 ppbv of gas-phase HNO_3, while particulate NO_y was detected from in situ measurements at flight altitude (Braun et al. 2019; H. Ziereis et al. 2019, unpublished manuscript). Particle NO_y was detected during four episodes over Spitzbergen, close to Iceland, and close to the Norwegian coast covering a total time span of about 2.5 h. More details are given in the "Highlighted results" section of the main text (Fig. 14). Data from a coincident ozone sonde launched from Ny-Ålesund was used for validation of ozone retrieved from GLORIA limb imager spectra (see Fig. 7 in main text).

PGS-09—22 January 2019: PSC hunting in cold vortex air and comparison between the airborne and spaceborne lidars WALES and CALIOP. HALO was heading toward the cold pool east of Greenland to measure PSCs, to probe regions with a high tropopause and $T < T_{NAT}$ and to fly along two overpass tracks of *CALIPSO* in the North Atlantic. The flight routes (Fig. ES4) were calculated such that the advection of air masses observed by CALIOP were considered. Cold air down to –72°C was encountered at flight altitude. HALO passed its most northern latitude at 1239 UT, with high-tropopause features visible in low O_3 and high N_2O. FL 450 was reached at 1321 UT at the most western point east of Canada. Here, enhanced nitric acid suggested previous vertical redistribution of HNO_3 by PSCs. At this point, the second flight track along the *CALIPSO* overpass started. The high-spectral-resolution capability of the WALES lidar enabled the determination of the lidar-ratio at 532-nm wavelength for different types of PSCs, a quantity needed by the retrieval algorithm of simpler backscatter lidars. Again, particles were observed above HALO flight altitude by WALES, some of them with enhanced backscatter and low depolarization ratios, suggesting supercooled ternary solution (STS) droplets at the lower altitudes and ice PSCs above. The WALES lidar detected an ice PSC with a horizontal extension of more than 1400 km (Voigt et al. 2018). The ice PSC extended between 18- and 24-km altitude and was most likely surrounded by nitric acid

trihydrate (NAT), supercooled ternary solution (STS) droplets, and particle mixtures (Voigt et al. 2018). The PSC observations of WALES and the comparisons to the CALIOP matches are discussed in the "Highlighted results" section of the main text (Figs. 11 and 12).

Six dropsondes were released between 80° and 75°N to sample a polar low with double tropopauses underneath HALO flight altitude. Very fine structured, inhomogeneous stratospheric air was sampled along the track back to the Norwegian coast. A detour to the Finish boarder at FL 480 was adjusted in flight to meet favorable gravity wave conditions in northern Scandinavia, accompanied by high nitric acid at flight level.

PGS-10—25 January 2019: Gravity wave research over Iceland. This flight (Fig. ES5) was primarily addressing a gravity wave situation over Iceland by applying

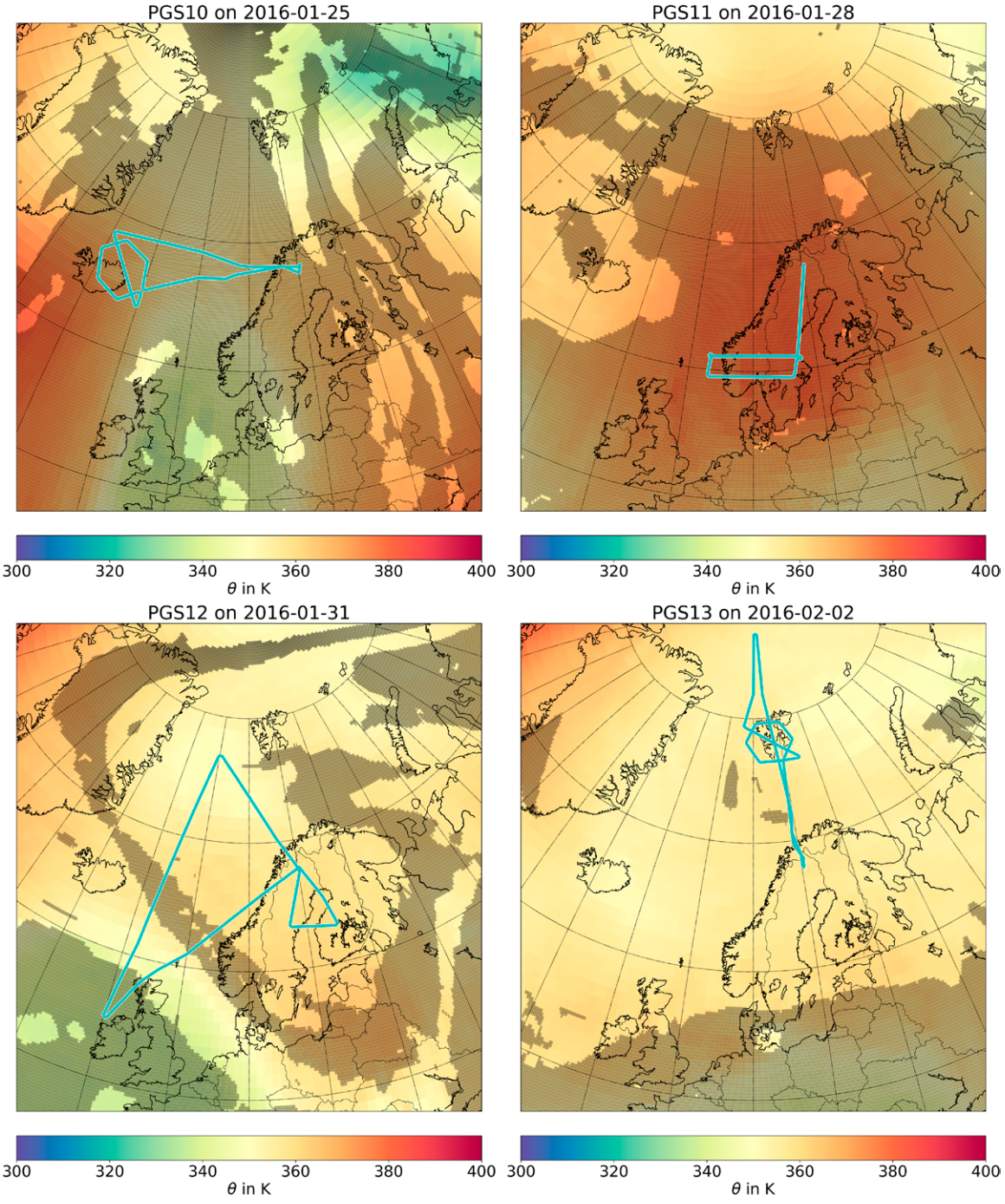

Fig. ES5. As in Fig. ES3, but for flights PGS-10–PGS-13.

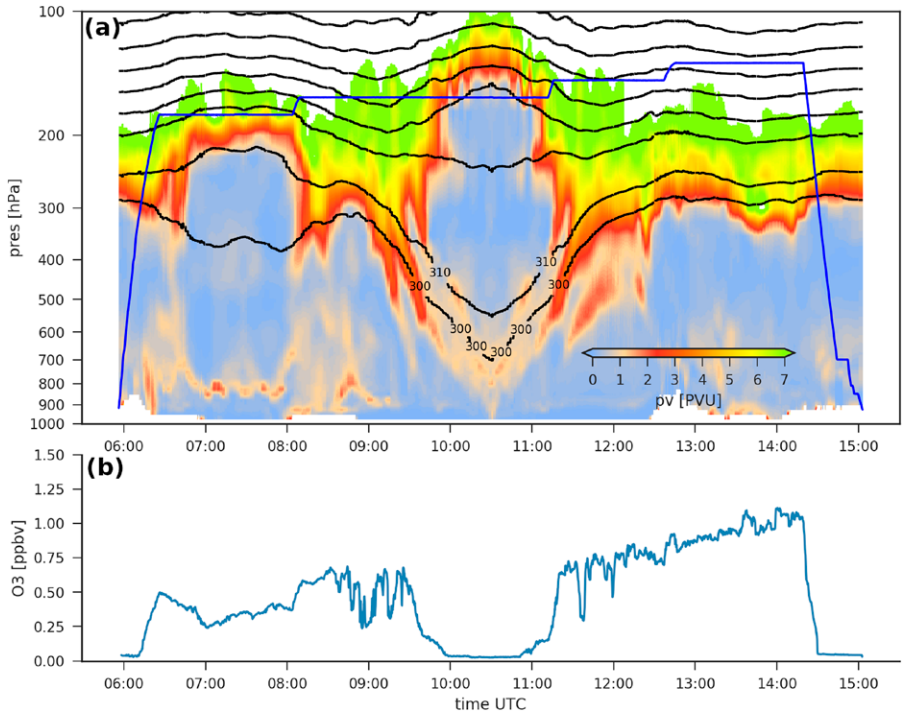

Fig. ES6. (a) Cross section of PV (PVU) along flight path of PGS-12 from ICON-ART forecast, illustrating the complex tropopause structure with the WCB close to the southern turning point (~1030 UTC) where the tropopause was reaching up to FL 450. Black contour lines represent the potential temperature in steps of 10 K. The blue line represents the flight altitude (hPa). The simulation was initialized from ECMWF IFS forecast at 0000 UTC. The interpolation was performed on the triangular ICON grid using a nearest-neighbor interpolation. (b) FAIRO measurements of ozone illustrating the WCB with very low ozone around the turning point and the filamentation at the northern edge of the jet stream.

a hexagon-shaped flight path for tomographic measurements of the target region with the limb imager GLORIA (Ungermann et al. 2010, 2011). Dropsondes were released in the target region for temperature comparison with GLORIA measurements. Over Iceland the cruise took place at constant flight level and six dropsondes were dropped every 8 min, starting from the crossing line of the lag with the northwestern leg of the hexagon. From this time on, gravity wave structures could be measured by the trace gas instruments and GLORIA and wave structures could also be seen by eye from the aircraft. A detailed study of these first tomographic observations of gravity waves by infrared limb imaging was published by Krisch et al. (2017). Apart from this, particle NO_y was also detected at this flight during two time periods west of Norway with a total length of about 1 h (cf. Fig. 13 in main text).

PGS-11—28 January 2019: Coordinated flight with Falcon for mountain-wave research. The objective of this flight (Fig. ES5) was to explore a transient mountain-wave situation over southern Scandinavia with coordinated flights of the research aircrafts HALO and Falcon. Flights were coordinated along elongated, straight cross-mountain legs, with the goal to determine the energy and momentum fluxes at different flight levels simultaneously, to explore tropopause structure by in situ and remote sensing instruments, and to observe mountain waves with GLORIA on higher flight legs. While Falcon was flying at FL 340 looking downward with the wind-lidar, HALO stayed at FL 270 probing the highly variable tropopause water vapor structure with WALES quasi simultaneously. The horizontal distance was approximately at 8 nautical miles (1 n mi = 1.852 km) between the aircraft. Clouds were encountered at flight level and above with enhanced-particle NO_y. After finishing the coordinated flight, Falcon returned to Kiruna and HALO climbed to FL430. Here HALO turned south and probed on a parallel leg the gravity wave with GLORIA. Temperature fluctuations of up to 4 K were measured in situ. The last leg was performed at FL 450, again with noticeable turbulence and large variabilities in the trace gases (cf. O_3 and HNO_3).

PGS-12—31 January 2016: Late January survey and iso-SZA flight for test of chlorine/bromine chemistry. The flight PGS-12 (Fig. ES5) had three major objectives: 1) a late January survey with expected PSCs along most of the flight path in Arctic stratospheric air, 2) probing of subtropical air at the southernmost tip of the route after crossing a strong jet stream over Ireland associated with a warm conveyor belt (WCB), and 3) a section of the flight enabling constant solar zenith angle (SZA) to investigate chlorine/bromine chemistry by DOAS UV–VIS observations.

Measurements revealed extensively nitrified layers up to about 8 ppbv of gaseous NO_y in Arctic vortex air

masses at upper flight levels (with high ozone VMRs at 800 ppbv and higher) and large reactive chlorine (Cl_y up to 1 ppbv, as deduced from CFC-12 tracer measurements). PSCs (presumably NAT and STS, no ice) were observed on the outbound legs to 77°N and on the southbound leg to Ireland, but being fainter and shallower than on the flights before. Above the WCB however, strong thick PSCs were encountered almost directly above the cirrus clouds, likely due to uplifting and adiabatic cooling of air in the WCB. When passing the jet north of the WCB over Ireland, wind speeds up to 200 kt were registered along with turbulence. Inside the WCB, cirrus clouds were encountered with particles containing NO_y. The WBC was characterized by very clean marine air with extremely low amounts of gas-phase NO_y and ozone (see Fig. ES6). The transition region between the WCB and the lowermost stratosphere was strongly filamented with ozone mixing ratios changing by several hundred parts per billion by volume within tens of kilometers.

Results from the iso-SZA flight leg are discussed in the "Highlighted results" section of the main text (Fig. 17).

PGS-13—2 February 2016: End of Phase 2 survey underneath cold pool and gravity waves over Spitsbergen. The flight PGS-13 (Fig. ES5) provided a high-latitude survey underneath the still-existing cold pool along long transects from 67° to 87°N with temperatures as low as 196 K at 150 hPa and 189 K at 50 hPa. The whole flight was inside the Arctic polar vortex centered at 150 hPa over northern Scandinavia. By this, the state and composition of the Arctic LMS along PSCs were probed finishing up campaign phase 2. In addition, a gravity wave situation over Svalbard was explored with tomographic measurements by GLORIA and dropsondes released for temperature comparisons.

Mission phase 3: Late winter–spring. PGS-14–26 February 2019: First flight after the break: Accessing strongly subsided vortex air masses over Baffin Island. The forecast maps indicated an area of strongly subsided air masses with potential temperatures as high as about 400 K at flight level, which was not reachable before. A long flight (Fig. ES7) was planned in this situation to provide a late February survey at different potential temperature levels. The strongly subsided air masses between Greenland and Canada were characterized by low N_2O, high DO_3, ClO_x, DNO_y, and $ClONO_2$. A detailed discussion of this flight with

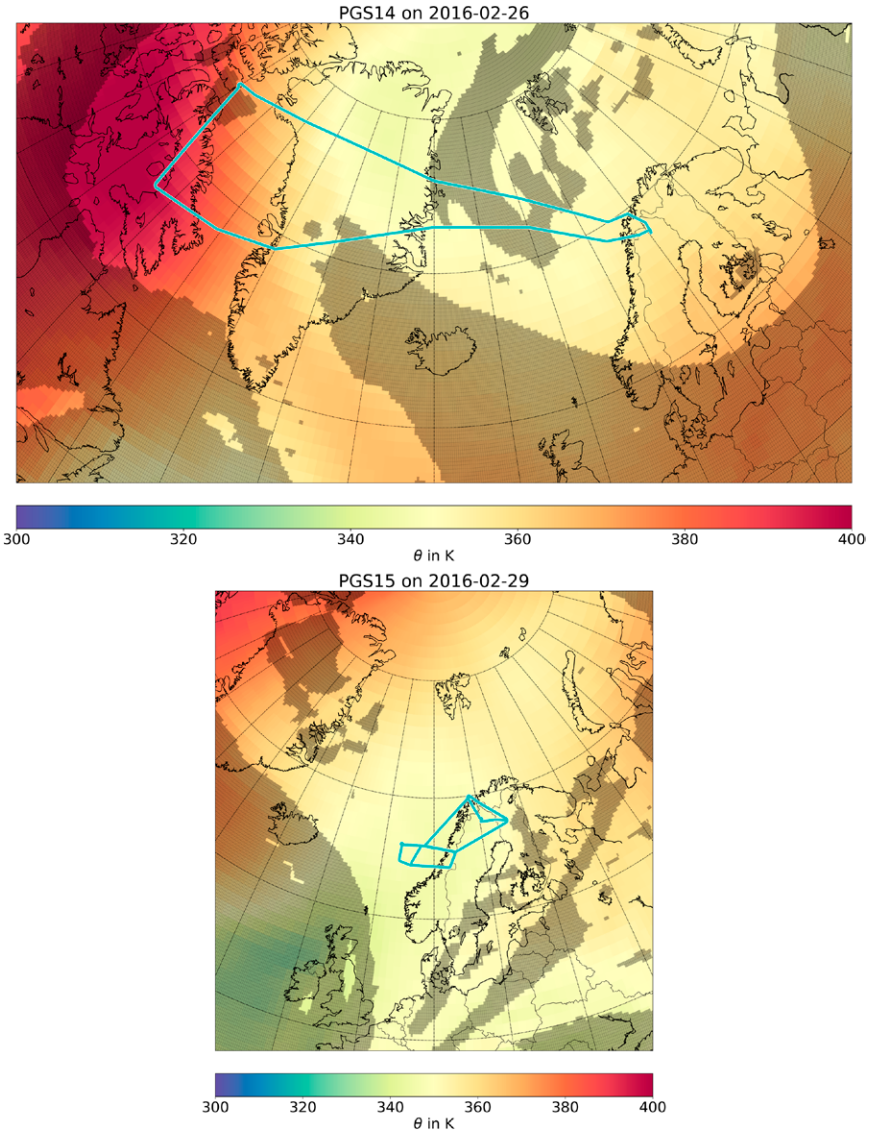

Fig. ES7. As in Fig. ES3, but for flights PGS-14 and PGS-15.

respect to chlorine species is given in the "Highlighted results" section of the main text (Fig. 15).

PSCs were present during the whole Atlantic overpass. During the southward leg over Baffin Island strongly subsided air masses were measured with volume mixing ratios of over 1200 ppb for ozone (FAIRO), 203 ppb for N_2O (TRIHOP), and 7.05 ppt for SF_6 (GhOST). Ambient air was relatively warm at –39°C.

PGS-15—29 February 2016: Probing a polar low and gravity waves in northern Scandinavia. The days before this flight (Fig. ES7), a very confined polar low moved from the east coast of Greenland toward Scandinavia. Associated to that, gravity waves occurred above Scandinavia. The situation was probed mainly by in situ instruments at five different flight levels.

The first flight leg at FL300 was performed to probe gravity waves with in situ measurements. Tropospheric tracers (CO and SO_2) were simultaneously enhanced in this region. Above HALO cloud structures were seen with WALES. The transfer toward the polar low with a PV anomaly with a low tropopause was done at FL 380. Three dropsondes were dropped into and near the polar low to probe the vertical structure.

Afterward, at FL 240 the polar low associated with a tropopause fold was probed by the WALES lidar and in situ instruments. Stratospheric tracers (HCl, O_3, and HNO_3) were enhanced inside the predicted region. Clouds were encountered at the eastern end of the leg, here in combination with tropospheric tracers. The second leg was preformed south of the polar low at FL 430 to probe the structure with GLORIA. The third leg at FL 300 was matched with the first leg for in situ measurements inside the fold. Similar structures as during the lower leg were found with different magnitudes in the tropospheric and stratospheric tracers. The fourth leg was again used for GLORIA measurements at FL 450.

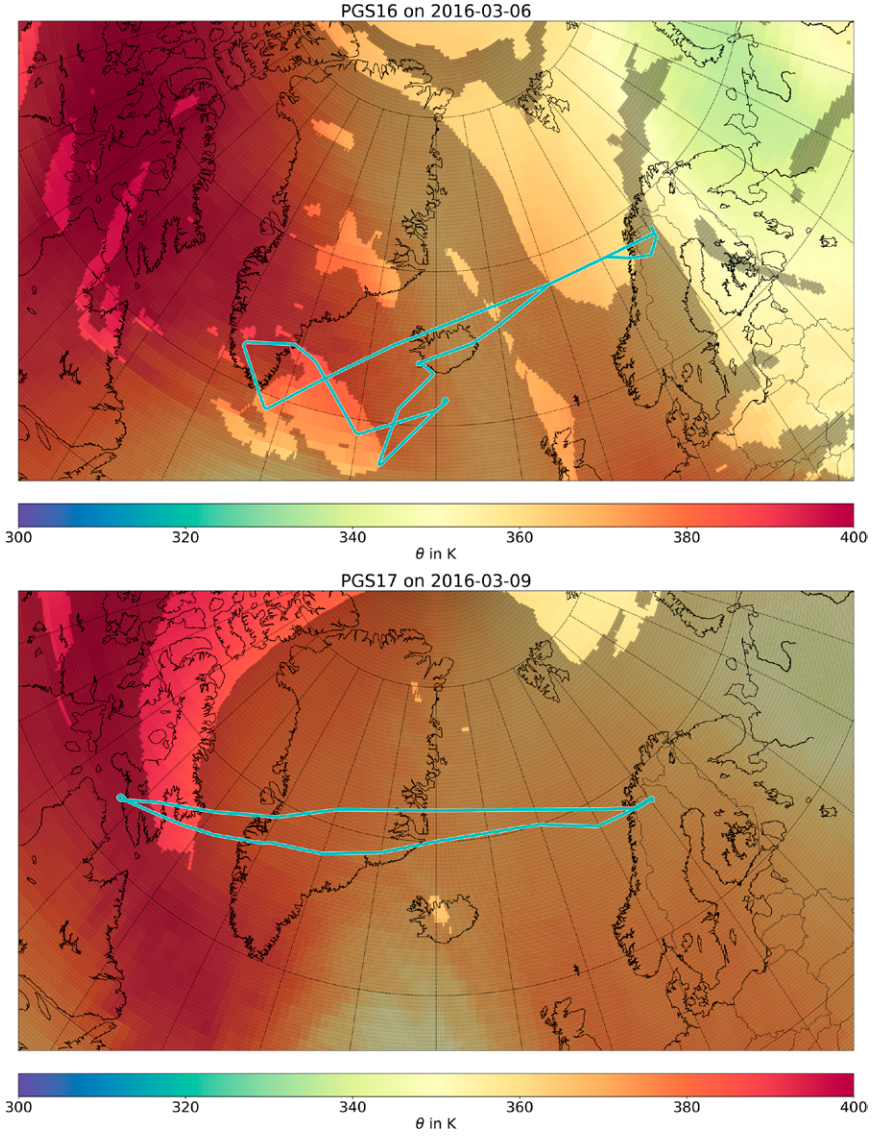

Fig. ES8. As in Fig. ES3, but for flights PGS-16 and PGS-17.

PGS-16—6 March 2016: Gravity Wave research over Greenland combined with filaments south of Iceland. A gravity wave situation triggered by the Southern tip of Greenland was the primary focus of the flight (Fig. ES8). In addition, subsided air masses with low N_2O and potential high O_3 loss at different flight levels south of Iceland were to be probed and on way back high-altitude cirrus clouds at FL360 over Kiruna to be observed. The rather complicated flight route

with several maneuvers and different flight levels was realized by implementing a fuel stop in Keflavik, Iceland.

PGS-17—9 March 2016: Second flight to Baffin Bay to probe aged subsided vortex air. About two weeks after PGS-14 this was the second time to probe the aged-vortex air masses with high potential temperature between Canada and Greenland (Fig. ES8) with the goal to follow up the development of the subsidence, and the fate of high NO_y and chlorine with potential high ozone loss. To achieve high flight levels in the target region a stopover in Kangerlussuaq, Greenland, was implemented.

PGS-18—10 March 2016: Gravity wave observations over northwestern Greenland, last local flight from Kiruna. Another gravity wave situation over northwest Greenland was explored during this flight (Fig. ES9). Strongly filamented air masses between Scandinavia and Greenland were in the focus with measurements at different flight levels.

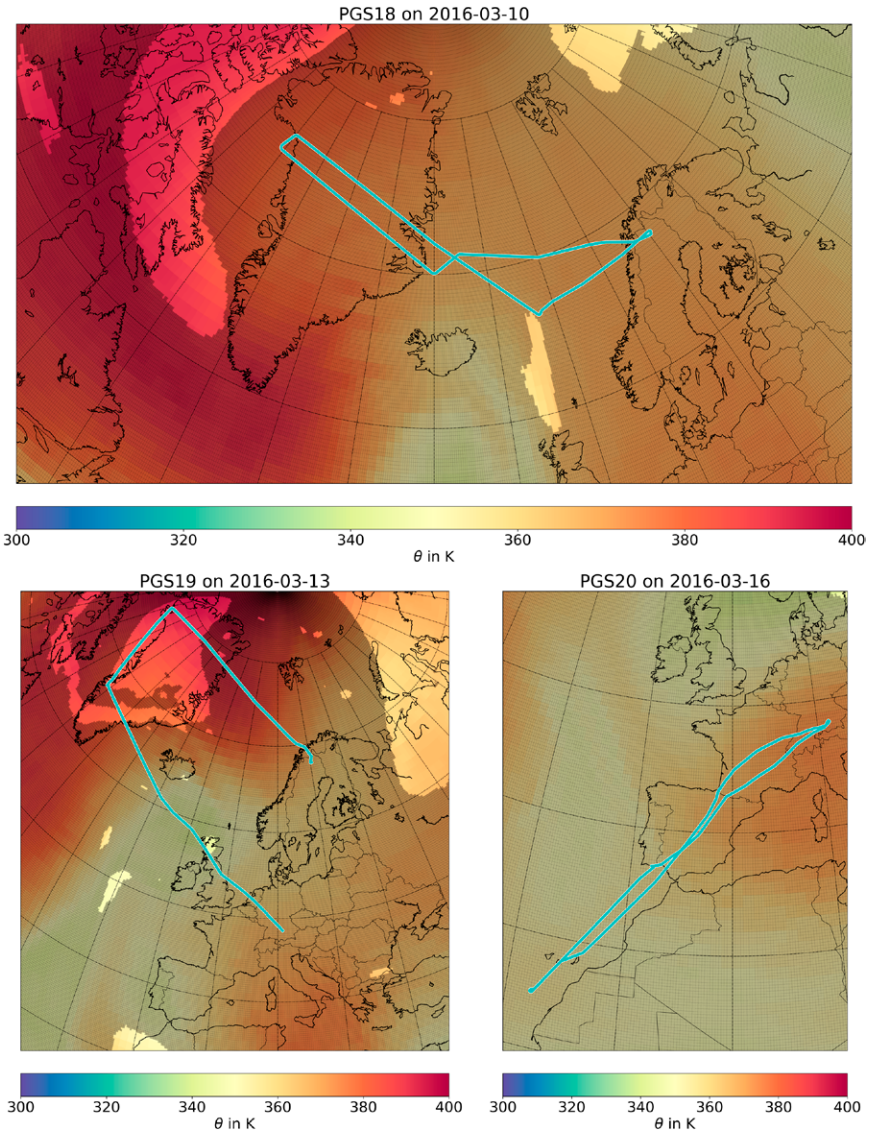

Fig. ES9. As in Fig. ES3, but for flights PGS-18–PGS-20.

PGS-19—13 March 2016: Transfer flight back to Oberpfaffenhofen via Greenland. The transfer flight back to Germany (Fig. ES9) was used to probe once again the aged-vortex air masses that were still situated between Greenland and Canada. A stopover in in Kangerlussuaq was necessary to reach larger distances and a higher ceiling altitude at the region of interest. On the way back to Germany, the tropopause was crossed at high altitude indicating subtropical air masses. Patches of enhanced HNO_3 were measured by GLORIA down to about 8 km (see Johansson et al. 2018; Braun et al. 2019).

PGS-20—16 March 2016: Southbound survey flight (SALSA-2). The goal of this second SALSA flight was to horizontally cross the tropopause at a high altitude and access a wide range of equivalent latitudes on the way from the middle latitudes to the subtropics. The flight route (Fig. ES9) went from Oberpfaffenhofen (48°N) to the Canary Islands (25°N) with a fuel stop in Faro, Portugal. On both flight legs, filaments of a stratospheric streamer with polar characteristics were crossed over southern France.

PGS-21—18 March 2016: Match flight for air masses probed during PGS-19. Vortex remnants still existing over northern Scandinavia motivated us for a flight (Fig. ES10) to probe once again polar vortex air masses

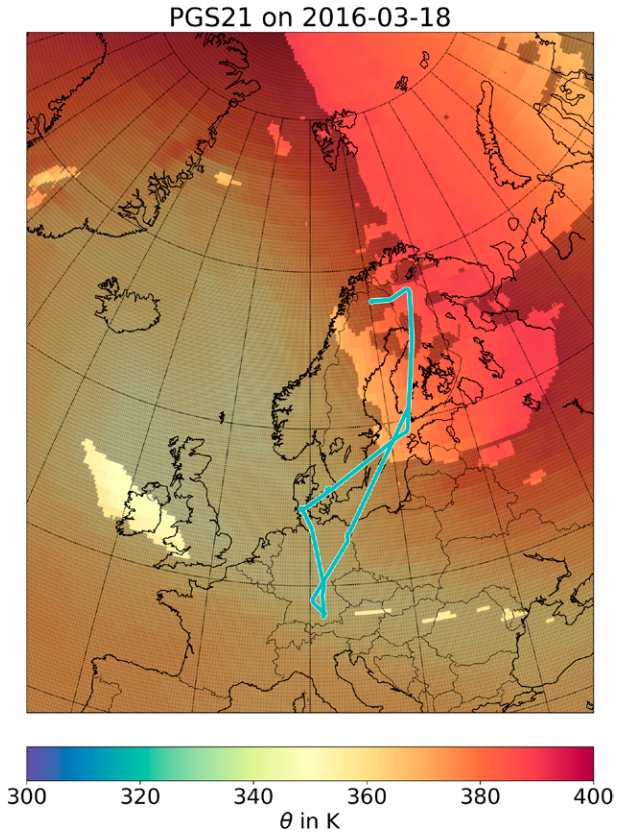

Fig. ES10. As in Fig. ES3, but for flight PGS-21.

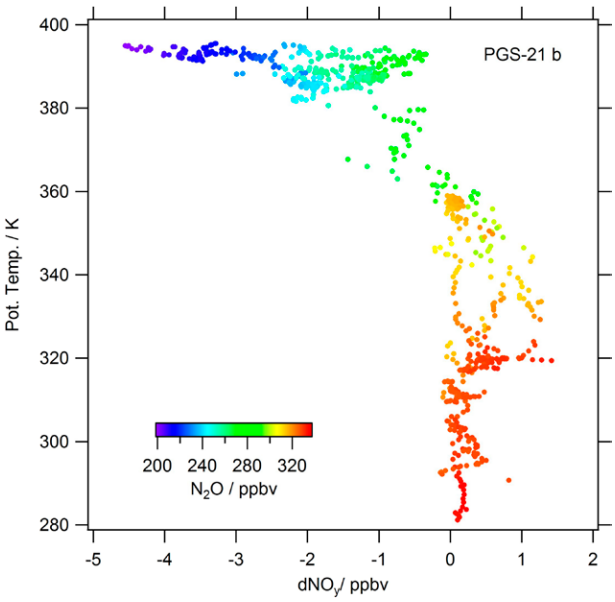

Fig. ES11. DNO_y derived from the N_2O–NO_y relation vs potential temperature for the PGS-21 flight on 18 Mar 2016, based on AENEAS (NO_y) and TRIHOP (N_2O) measurements. The N_2O mixing ratio is color coded. Denitrification is still significant above about 360 K, while excess NO_y is seen in the LMS at lower altitudes.

that had been probed 5 days ago on PGS-19 over Greenland. In addition, cirrus clouds were studied in situ at FL380 and remotely with the lidar. Patches of enhanced HNO_3 were still present down to about 340 K as measured by GLORIA (see Fig. 16c in main text and Johansson et al. 2018; Braun et al. 2019). Diagnostics of DNO_y based on in situ measurements of NO_y and N_2O is shown in Fig. ES11.

APPENDIX: LIST OF ABBREVIATIONS AND ACRONYMS.

ACE-FTS	Atmospheric Chemistry Experiment–Fourier Transform Spectrometer
AENEAS	Atmospheric Nitrogen Oxides Measuring System
AIMS	Atmospheric Ionization Mass Spectrometer
BAHAMAS	Basic HALO Measurement and Sensor System
CALIOP	Cloud-Aerosol Lidar with Orthogonal Polarization
CALIPSO	*Cloud–Aerosol Lidar and Infrared Pathfinder Satellite Observations*
CLaMS	Chemical Lagrangian Model of the Stratosphere
DLR	German Aerospace Center
ECD	Electron Capture Dissociation
ECMWF	European Centre for Medium-Range Weather Forecasts
EMAC	ECHAM–MESSy Atmospheric Chemistry Model
FAIRO	Fast and Accurate In Situ Ozone Instrument
FISH	The Fast In Situ Stratospheric Hygrometer
FL	Flight level
GC	Gas chromatography
GhOST-MS	Gas Chromatograph for the Observation of Stratospheric Tracers–Mass Spectrometer
GLORIA	Imaging Fourier Transform Infrared Spectrometer
GW-LCYCLE	Gravity Wave Life Cycle Experiment
HAGAR	High Altitude Gas Analyzer
HAI	Hygrometer for atmospheric investigations

HALO	High Altitude and Long Range Research Aircraft
ICON-ART	Icosahedric Non-Hydrostatic Model for Aerosols and Reactive Trace Gases
IFTS	Imaging Fourier Transform Spectroscopy
KIT	Karlsruhe Institute of Technology
LMS	Lowermost stratosphere
Mini-DOAS	Miniaturized differential optical absorption spectroscopy
ML-CIRRUS	Midlatitude Cirrus experiment
MLS	Microwave Limb Sounder
MS	Mass spectrometer
NAT	Nitric acid trihydrate
PGS	POLSTRACC/GW-LCYCLE/SALSA
POLSTRACC	Polar Stratosphere in a Changing Climate
PV	Potential vorticity
SALSA	Seasonality of Air Mass Transport and Origin in the Lowermost Stratosphere using HALO Aircraft
STS	Supercooled ternary solutions
SZA	Solar zenith angle
TACTS/ESMVal	Transport and Composition in the Upper Troposphere/Lowermost Stratosphere/Earth System Model Validation
TDL	Tunable diode laser
UTC	Universal Time, Coordinated
UTLMS	Upper troposphere/lowermost stratosphere
UTLS	Upper troposphere/lower stratosphere
WALES	Multi-wavelength H_2O/O_3 differential absorption lidar
WARAN	Water Vapor Analyzer
WCB	Warm conveyor belt
WISE	Wave-driven isentropic exchange HALO campaign

REFERENCES

Bönisch, H., A. Engel, T. Birner, P. Hoor, D. W. Tarasick, and E. A. Ray, 2011: On the structural changes in the Brewer-Dobson circulation after 2000. *Atmos. Chem. Phys.*, **11**, 3937–3948, https://doi.org/10.5194/acp-11-3937-2011.

Braun, M., and Coauthors, 2019: Nitrification of the lowermost stratosphere during the exceptionally cold Arctic winter 2015/16. *Atmos. Chem. Phys. Discuss.*, https://doi.org/10.5194/acp-2019-108.

Buchholz, B., A. Afchine, A. Klein, C. Schiller, M. Krämer, and V. Ebert, 2017: HAI, a new airborne, absolute, twin dual-channel, multi-phase TDLAS-hygrometer: Background, design, setup, and first flight data. *Atmos. Meas. Tech.*, **10**, 35–57, https://doi.org/10.5194/amt-10-35-2017.

Burkholder, J. B., and Coauthors, 2015: Chemical kinetics and photochemical data for use in atmospheric studies. Evaluation 18, JPL Publ. 15-10, Jet Propulsion Laboratory, 1392 pp., http://jpldataeval.jpl.nasa.gov.

Deutschmann, T., and Coauthors, 2011: The Monte Carlo atmospheric radiative transfer model McArtim: Introduction and validation of Jacobians and 3-D features. *J. Quant. Spectrosc. Radiat. Transfer*, **112**, 1119–1137, https://doi.org/10.1016/j.jqsrt.2010.12.009.

Engel, A., and Coauthors, 2006: Highly resolved observations of trace gases in the lowermost stratosphere and upper troposphere from the Spurt project: An overview. *Atmos. Chem. Phys.*, **6**, 283–301, https://doi.org/10.5194/acp-6-283-2006.

Friedl-Vallon, F., and Coauthors, 2014: Instrument concept of the imaging Fourier transform spectrometer GLORIA. *Atmos. Meas. Tech.*, **7**, 3565–3577, https://doi.org/10.5194/amt-7-3565-2014.

Grooß, J.-U., and Coauthors, 2014: Nitric acid trihydrate nucleation and denitrification in the Arctic stratosphere. *Atmos. Chem. Phys.*, **14**, 1055–1073, https://doi.org/10.5194/acp-14-1055-2014.

Hüneke, T., and Coauthors, 2017: The novel HALO mini-DOAS instrument: Inferring trace gas concentrations from airborne UV/visible limb spectroscopy under all skies using the scaling method. *Atmos. Meas. Tech.*, **10**, 4209–4234, https://doi.org/10.5194/amt-10-4209-2017.

Johansson, S., and Coauthors, 2018: Airborne limb-imaging measurements of temperature, HNO_3, O_3, $ClONO_2$, H2O and CFC-12 during the Arctic winter 2015/2016: Characterization, in-situ validation and

comparison to Aura/MLS. *Atmos. Meas. Tech.*, **11**, 4737–4756, https://doi.org/10.5194/amt-11-4737-2018.

Jurkat, T., and Coauthors, 2010: Airborne stratospheric ITCIMS measurements of SO_2, HCl, and HNO_3 in the aged plume of volcano Kasatochi. *J. Geophys. Res.*, **115**, D00L17, https://doi.org/10.1029/2010JD013890.

——, and Coauthors, 2014: A quantitative analysis of stratospheric HCl, HNO_3, and O_3 in the tropopause region near the subtropical jet. *Geophys. Res. Lett.*, **41**, 3315–3321, https://doi.org/10.1002/2013GL059159.

——, S. Kaufmann, C. Voigt, D. Schäuble, P. Jeßberger, and H. Ziereis, 2016: The airborne mass spectrometer AIMS – Part 2: Measurements of trace gases with stratospheric or tropospheric origin in the UTLS. *Atmos. Meas. Tech.*, **9**, 1907–1923, https://doi.org/10.5194/amt-9-1907-2016.

——, and Coauthors, 2017: Depletion of ozone and reservoir species of chlorine and nitrogen oxide in the lower Antarctic polar vortex measured from aircraft. *Geophys. Res. Lett.*, **44**, 6440–6449, https://doi.org/10.1002/2017GL073270.

Kaufmann, S., C. Voigt, P. Jeßberger, T. Jurkat, H. Schlager, A. Schwarzenboeck, M. Klingebiel, and T. Thornberry, 2014: In-situ measurements of ice saturation in young contrails. *Geophys. Res. Lett.*, **41**, 702–709, https://doi.org/10.1002/2013GL058276.

——, and Coauthors, 2016: The airborne mass spectrometer AIMS – Part 1: AIMS-H2O for UTLS water vapor measurements. *Atmos. Meas. Tech.*, **9**, 939–953, https://doi.org/10.5194/amt-9-939-2016.

——, and Coauthors, 2018: Intercomparison of midlatitude tropospheric and lower stratospheric water vapor measurements and comparison to ECMWF humidity data. *Atmos. Chem. Phys.*, **18**, 16 729–16 745, https://doi.org/10.5194/acp-2018-744

Krause, J., and Coauthors, 2018: Mixing and ageing in the polar lower stratosphere in winter 2015/2016. *Atmos. Chem. Phys.*, **18**, 6057–6073, https://doi.org/10.5194/acp-2017-955.

Krautstrunk, M., and A. Giez, 2012: The transition from FALCON to HALO era airborne atmospheric research. *Atmospheric Physics*, U. Schumann, Ed., Springer, 609–624, https://doi.org/10.1007/978-3-642-30183-4_37.

Krisch, I., and Coauthors, 2017: First tomographic observations of gravity waves by the infrared limb imager GLORIA. *Atmos. Chem. Phys.*, **17**, 14 937–14 953, https://doi.org/10.5194/acp-17-14937-2017.

Lelieveld, J., and Coauthors, 2018: The South Asian monsoon—Pollution pump and purifier. *Science*, **361**, 270–273, https://doi.org/10.1126/science.aar2501.

Livesey, N. J., and Coauthors, 2018: Version 4.2x Level 2 data quality and description document. Tech. Rep. JPL D-33509 Rev. D, Jet Propulsion Laboratory, 169 pp., https://mls.jpl.nasa.gov/data/v4-2_data_quality_document.pdf.

Marsing, A., and Coauthors, 2019: Chlorine partitioning in the lowermost Arctic vortex during the cold winter 2015/2016. *Atmos. Chem. Phys.*, **19**, 10 757–10 772, https://doi.org/10.5194/acp-19-10757-2019.

Meyer, J., and Coauthors, 2015: Two decades of water vapor measurements with the FISH fluorescence hygrometer: A review. *Atmos. Chem. Phys.*, **15**, 8521–8538, https://doi.org/10.5194/acp-15-8521-2015.

Müller, S., and Coauthors, 2016: Impact of the Asian monsoon on the extratropical lower stratosphere: Trace gas observations during TACTS over Europe 2012. *Atmos. Chem. Phys.*, **16**, 10 573–10 589, https://doi.org/10.5194/acp-16-10573-2016.

Nash, E. R., P. A. Newman, J. E. Rosenfield, and M. R. Schoeberl, 1996: An objective determination of the polar vortex using Ertel's potential vorticity. *J. Geophys. Res.*, **101**, 9471–9478, https://doi.org/10.1029/96JD00066, 1996.

Pitts, M. C., L. R. Poole, and R. Gonzalez, 2018: Polar stratospheric cloud climatology based on CALIPSO spaceborne lidar measurements from 2006 to 2017. *Atmos. Chem. Phys.*, **18**, 10 881–10 913, https://doi.org/10.5194/acp-18-10881-2018.

Rautenhaus, M., G. Bauer, and A. Dörnbrack, 2012: A web service based tool to plan atmospheric research flights. *Geosci. Model Dev.*, **5**, 55–71, https://doi.org/10.5194/gmd-5-55-2012.

Riese, M., and Coauthors, 2014: Gimballed Limb Observer for Radiance Imaging of the Atmosphere (GLORIA) scientific objectives. *Atmos. Meas. Tech.*, **7**, 1915–1928, https://doi.org/10.5194/amt-7-1915-2014.

Sala, S., H. Bönisch, T. Keber, D. E. Oram, G. Mills, and A. Engel, 2014: Deriving an atmospheric budget of total organic bromine using airborne in-situ measurements from the western Pacific area during SHIVA. *Atmos. Chem. Phys.*, **14**, 6903–6923, https://doi.org/10.5194/acp-14-6903-2014.

Stratmann, G., and Coauthors, 2016: NO and NO_y in the upper troposphere: Nine years of CARIBIC measurements onboard a passenger aircraft. *Atmos. Environ.*, **133**, 93–111, https://doi.org/10.1016/j.atmosenv.2016.02.035.

Stutz, J., and Coauthors, 2017: A new differential optical absorption spectroscopy instrument to study atmospheric chemistry from a high-altitude unmanned aircraft. *Atmos. Meas. Tech.*, **10**, 1017–1042, https://doi.org/10.5194/amt-10-1017-2017.

Ungermann, J., M. Kaufmann, L. Hoffmann, P. Preusse, H. Oelhaf, F. Friedl-Vallon, and M. Riese, 2010: Towards a 3-D tomographic retrieval for the airborne limb-imager GLORIA. *Atmos. Meas. Tech.*, **3**, 1647–1665, https://doi.org/10.5194/amt-3-1647-2010.

——, and Coauthors, 2011: A 3-D tomographic retrieval approach with advection compensation for the airborne limb-imager GLORIA. *Atmos. Meas. Tech.*, **4**, 2509–2529, https://doi.org/10.5194/amt-4-2509-2011.

Voigt, C., and Coauthors, 2014: Evolution of CO2, SO2, HCl, and HNO3 in the volcanic plumes from Etna. *Geophys. Res. Lett.*, **41**, 2196–2203, https://doi.org/10.1002/2013GL058974.

——, and Coauthors, 2017: ML-CIRRUS: The airborne experiment on natural cirrus and contrail cirrus with the high-altitude long-range research aircraft HALO. *Bull. Amer. Meteor. Soc.*, **98**, 271–288, https://doi.org/10.1175/BAMS-D-15-00213.1.

——, and Coauthors, 2018: Widespread polar stratospheric ice clouds in the 2015–2016 Arctic winter – Implications for ice nucleation. *Atmos. Chem. Phys.*, **18**, 15 623–15 641, https://doi.org/10.5194/acp-18-15623-2018.

Waters, J., and Coauthors, 2006: The Earth Observing System Microwave Limb Sounder (EOS MLS) on the Aura satellite. *IEEE T. Geosci. Remote*, **44**, 1075–1092, https://doi.org/10.1109/TGRS.2006.873771.

Werner, A., C. M. Volk, E. V. Ivanova, T. Wetter, C. Schiller, H. Schlager, and P. Konopka, 2010: Quantifying transport into the Arctic lowermost stratosphere. *Atmos. Chem. Phys,*. **10**, 11 623–11 639, https://doi.org/10.5194/acp-10-11623-2010.

Werner, B., and Coauthors, 2017: Probing the subtropical lowermost stratosphere and the tropical upper troposphere and tropopause layer for inorganic bromine. *Atmos. Chem. Phys.*, **17**, 1161–1186, https://doi.org/10.5194/acp-17-1161-2017.

Wirth, M., A. Fix, P. Mahnke, H. Schwarzer, F. Schrandt, and G. Ehret, 2009: The airborne multi-wavelength water vapor differential absorption lidar WALES: System design and performance. *Appl. Phys.*, **96B**, 201, https://doi.org/10.1007/s00340-009-3365-7.

Woiwode, W., and Coauthors, 2018: Mesoscale fine structure of a tropopause fold over mountains. *Atmos. Chem. Phys.*, **18**, 15 643–15 667, https://doi.org/10.5194/acp-18-15643-2018.

Zahn, A., J. Weppner, H. Widmann, K. Schlote-Holubek, B. Burger, T. Kühner, and H. Franke, 2012: A fast and precise chemiluminescence ozone detector for eddy flux and airborne application. *Atmos. Meas. Tech.*, **5**, 363–375, https://doi.org/10.5194/amt-5-363-2012.

Ziereis, H., H. Schlager, H. Fischer, C. Feigl, P. Hoor, R. Marquardt, and V. Wagner, 2000: Aircraft measurements of tracer correlations in the Arctic subvorter region during the Polar Stratospheric Aerosol Experiment (POLSTAR). *J. Geophys. Res.*, **105**, 24 305–24 313, https://doi.org/10.1029/2000JD900288.

——, and Coauthors, 2004: Uptake of reactive nitrogen on cirrus cloud particles during INCA. *Geophys. Res. Lett.*, **31**, L05115, https://doi.org/10.1029/2003GL018794.

Zöger, M., and Coauthors, 1999: Fast in situ stratospheric hygrometers: A new family of balloon-borne and airborne Lyman alpha photofragment fluorescence hygrometers. *J. Geophys. Res.*, **104**, 1807–1816, https://doi.org/10.1029/1998JD100025.